Appl. Magn. Reson. **3**, 257–281 (1992)

Applied Magnetic Resonance

Determination of Atomic Positions of Point Defects in Solids by ENDOR

J.-M.Spaeth

Fachbereich Physik, University of Paderborn, Paderborn, Germany

Received July 29, 1991

Abstract. The experimental results which are obtained from electron nuclear double resonance (ENDOR) of point defects in solids are briefly reviewed. From the relation between the experimental superhyperfine and quadrupole interaction tensors and the spin density distribution and charge density distribution, the details of the microscopic structure and thus the positions of atoms can in principle be obtained. For this, in general, a precise theory of the defect wave function is required. However, there are many cases in which simple approximations to the wave function can be used to determine atomic positions rather well. This is illustrated with several examples, mainly from ionic solids. The particular difficulties encountered in semiconductors and the influence of dynamical effects are also discussed.

1. Introduction

The determination of the precise microscopic structure of point defects in solids is an important task both in applied materials sciences and for their fundamental understanding. Many bulk properties of solids are controlled by a small number of defects with the consequence that their investigation and understanding is often of high technological relevance. Point defects play a key role in the large field of semiconductor physics with applications in micro-electronics and opto-electronics and in areas such as solid state lasers, X-ray scintillators, X-ray dosimetry and holography. There are many experimental methods to investigate the influence of point defects on the bulk properties, but not many to determine their microscopic structure. For electron microscopy they are too small, and there is no other imaging technique to investigate their structure. Electron paramagnetic resonance (EPR) methods have proved to be suitable methods with detailed information on the structure of paramagnetic point defects and thus their atomic positions can be obtained. However, the information obtained, albeit sometimes very detailed, is indirect in the sense that EPR spectra yield no "image", only infor-

mation on magnetic interactions between the magnetic moment of the unpaired electron or hole and magnetic moments of neighboring nuclei. With electron nuclear double resonance (ENDOR) these interactions can be resolved with many shells of neighbor nuclei giving the most detailed information on defect structure. With this information, the symmetry of a defect and the chemical identity of its constituents can often be determined. However, the atomic positions of the impurity (or "central" atom) and the relative distances of the constituents of a pair defect, or the lattice relaxation about an impurity remain unknown. In order to obtain this, in general, one needs the knowledge of the wave function of the defect, in principle a very precise knowledge from a spin unrestricted calculation. There are not many cases for which a sufficiently good wave function could be obtained. However, often one can use rather crude approximations to the wave functions to determine atomic positions. It is the aim of this contribution to briefly point out the nature and limitations of the experimental results one can obtain from ENDOR experiments and then to describe approximations to the wave functions which are useful – if applicable – to obtain atomic positions from the ENDOR data. This will generally be the case for ionic systems, in particular if precise ENDOR data of "distant" neighbors are available, which is illustrated with several examples. Defects in semiconductors such as Si and the III–V compounds present particular difficulties since exchange polarization effects of valence bands play an important role. An example of a recent calculation is presented which shows that "naive" inspection of the data and conclusions drawn from it do not give the right answer. Finally, when briefly discussing dynamical effects, a novel feature demonstrated recently is described. The entropy content of a defect determines its configuration which can change as a function of temperature.

2. ENDOR Experiments

Most ENDOR work in solids was done with the stationary ENDOR method introduced by Seidel [1]. The method is illustrated in Fig.1 for $S = 1/2$ and $I = 3/2$. In an ENDOR experiment one of the allowed EPR transitions ($\Delta m_S = \pm 1$, $\Delta m_I = 0$) is partly saturated, that is, the microwave power is taken high enough that the transition probability, $W_{MW} = \gamma B_1^2$, is of the order of (or larger than) the spin-lattice relaxation rate $W_{REL} = 1/T_1$. (Here γ is the gyromagnetic ratio of the electron, B_1 is the microwave field amplitude.) Under saturation, the spin population of the levels connected by the microwave transition deviates from thermal equilibrium (in the limit they become equally populated) resulting in a decrease of the EPR signal. The levels not connected by the EPR transition are not affected. Therefore, the population of the level $m_S = 1/2$, $m_I = +1/2$, for example, is now inverted with respect to the level $m_S = 1/2$, $m_I = -1/2$ (Fig.1). If these two levels are connected by an NMR transition, their level populations can be equalized

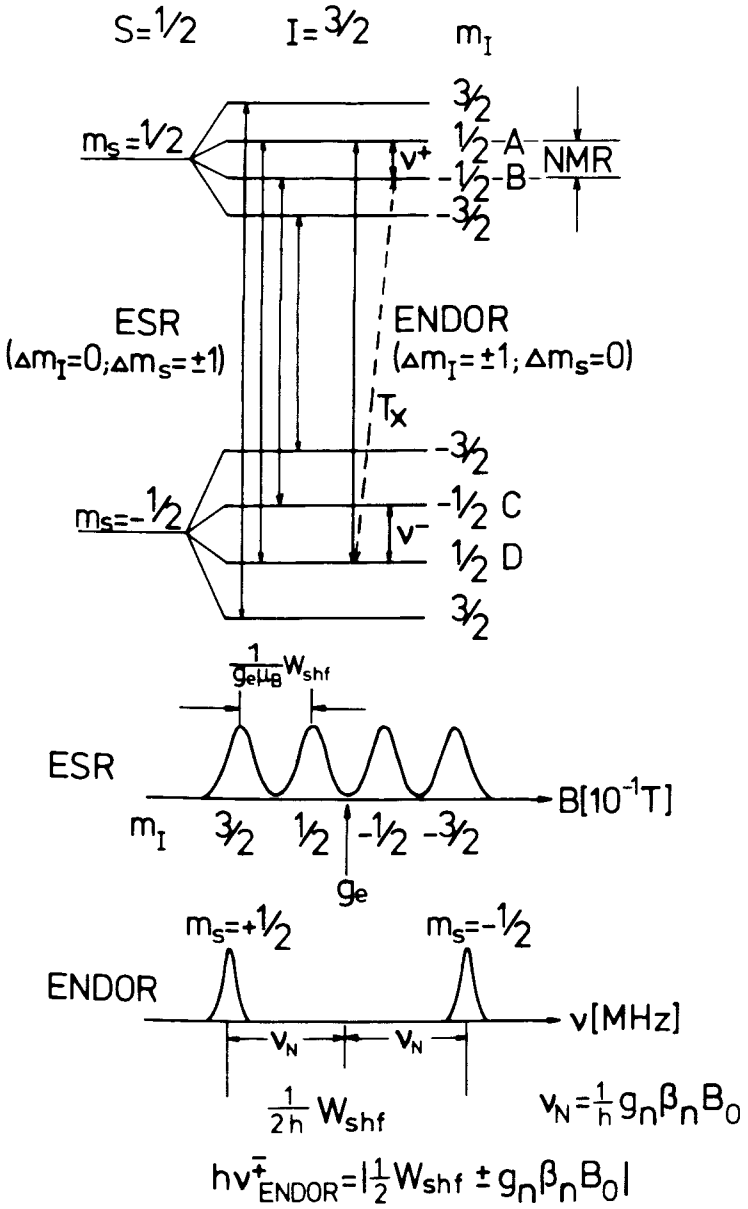

Fig.1. Energy-level diagram to explain the stationary electron nuclear double resonance (ENDOR) (see text).

which results in the population decrease of the $m_S = +1/2$, $m_I = +1/2$ level. This process leads to desaturation of the (partially) saturated transition $m_S = -1/2$, $m_I = +1/2$ to $m_S = +1/2$, $m_I = +1/2$, which is monitored. It occurs for two NMR frequencies since NMR frequencies for $m_S = 1/2$ and

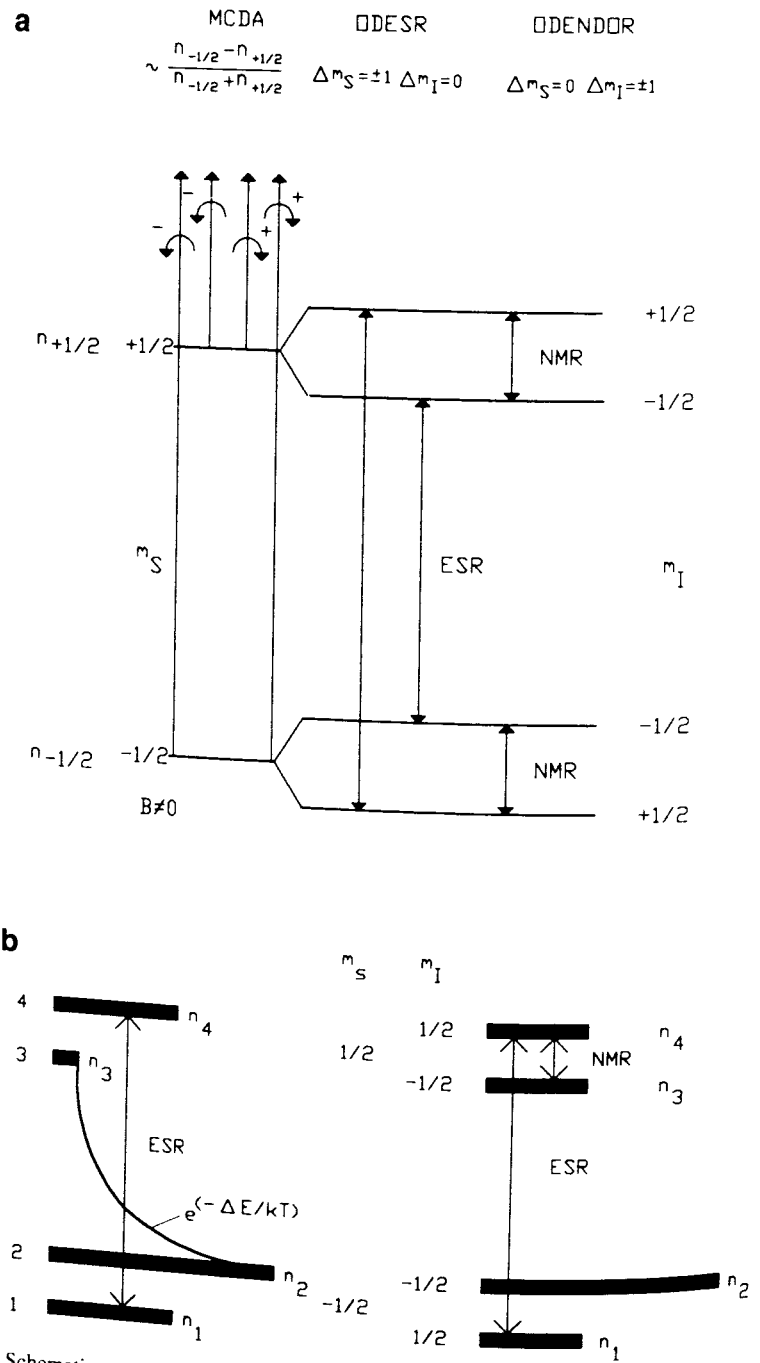

Fig.2. **a** Schematic explanation of optically detected paramagnetic resonance (ODEPR): The microwave-induced changes of the magnetic circular dichroism of the optical absorption (MCDA) are monitored. **b** Schematic explanation of optically detected electron nuclear double resonance (ODENDOR) using the MCDA technique (see text).

$m_S = -1/2$ are different (see below). A cross relaxation T_x allows the stationary observation of the desaturation. If several nuclei with the same or similar interactions are coupled to the unpaired electron, then the EPR pattern becomes complicated and the superhyperfine (shf) structure is usually not resolved. In ENDOR all nuclei with the same interaction give rise to only two (for $S = 1/2$) ENDOR lines, which greatly enhances the resolution. In ENDOR very weak interactions with distant ligand nuclei can be resolved.

Recently the optical detection of ENDOR using the optical absorption of a defect has proved to be a powerful method both in ionic solids and in particular in semiconductors [2,3]. The observation is based on changes induced into the magnetic circular dichroism of the optical absorption spectrum (MCDA) by EPR and NMR transitions. Fig.2a shows the principle of the ODEPR detection [4]. The MCDA is proportional to the spin polarization of the ground state. For $S = 1/2$ one obtains

$$\text{MCDA} \propto \frac{n_{-1/2} - n_{1/2}}{n_{-1/2} + n_{1/2}} . \tag{1}$$

Upon saturating EPR transitions, the MCDA is decreased, which is monitored. Fig.2b illustrates how an ENDOR transition can be observed for the simple case of $S = 1/2$, $I = 1/2$. In Fig.2b the abscissa gives the relative occupation of the levels. When saturating the EPR transition between levels 1 and 4, the MCDA can be diminished only by about 50 % of its value at thermal equilibrium. The MCDA signal observed is proportional to $n_2 - n_3$. If now an additional strong NMR transition is induced between levels n_4 and n_3, then the occupancy of these levels is also equalized. The saturating EPR transition is still present with the result that the occupation of all the three levels n_4, n_3 and n_1 are equal. However, the occupation of level n_3 is now bigger compared to the situation before the NMR transition was induced, whereas the occupancy of n_2 remains unchanged. The MCDA, still proportional to $n_2 - n_3$, is now reduced. Thus the NMR transition is indirectly detected by the optical detection of the spin polarization as an additional decrease of the MCDA signal measured when only saturating an EPR transition.

The advantage of the optical detection is high selectivity, when many defects are present simultaneously since their optical absorption bands usually are not identical, and sometimes, an enhanced sensitivity of several order of magnitude as compared to conventional ENDOR. Conventional ENDOR often required advanced methods such as ENDOR-induced EPR and double ENDOR methods be applied to separate ENDOR spectra of different defects with overlapping EPR spectra (see e.g. [5] and further references therein).

3. Analysis of ENDOR Spectra

Besides the shf interaction for nuclei with $I > 1/2$, there is usually also a nuclear quadrupole interaction. This interaction is due to the interaction between the electrical field gradient at the site of a nucleus and its nuclear quadrupole moment. In general the spin Hamiltonian describing the ENDOR spectrum is:

$$\mathcal{H} = g_e \beta_e B_0 \cdot \mathbf{S} + \sum_l (\mathbf{S} \cdot \tilde{A}_l \cdot \mathbf{I}_l - g_{n,l} \beta_n B_0 \cdot \mathbf{I}_l + \mathbf{I}_l \cdot \tilde{Q}_l \cdot \mathbf{I}_l) . \quad (2)$$

The sum runs over all nuclei interacting with the unpaired electron. For simplicity it is assumed that g_e is isotropic which is not the case in general. In Eq.(2) β_e is the Bohr magneton, B_0 is the static magnetic field, $g_{n,l}$ is the nuclear g-factor of nucleus l and β_n is the nuclear magneton. **S** and **I** are the electron and nuclear spin operators, respectively. The shf tensor $\tilde{A}$ is often decomposed into an isotropic and an anisotropic part according to

$$\tilde{A} = a \cdot \tilde{1} + \tilde{B} , \quad (3)$$

$$b = \frac{1}{2} B_{zz} , \quad (4)$$

$$b' = \frac{1}{2} (B_{xx} - B_{yy}) . \quad (5)$$

Here x, y, z is the principal axis system of the shf tensor. Parameter a is the isotropic shf constant (Fermi contact term). The diagonal elements of $\tilde{B}$ can be used to define b and b', where b is the anisotropic shf constant and b' describes the deviation of the tensor from axial symmetry, as follows: The largest interaction is along the z direction. $\tilde{Q}$ is the traceless quadrupole interaction tensor with the elements

$$q_{ik} = \frac{e Q_l}{2I(2I-1)} \frac{\partial^2 V}{\partial x_i \partial x_k} \Big|_{r=0} , \quad (6)$$

where Q_l is the quadrupole moment of nucleus l, V is the electrical potential. The spectra are usually analyzed in terms of the quadrupole interaction constants:

$$q = \frac{1}{2} Q_{zz} , \quad (7)$$

$$q' = \frac{1}{2}(Q_{xx} - Q_{yy}) \,. \tag{8}$$

If the shf and quadrupole interactions are small compared to the electron Zeeman term, then the quantization of the electron spin is not affected by these interactions and the nuclei are independent of each other. They can be treated separately and the sum in Eq.(2) can be omitted. In perturbation theory to first order, that is with the conditions

$$B_{ik}, Q_{ik} \ll \left| a \pm \frac{1}{m_S} g_n \beta_n B_0 \right| \,, \tag{9}$$

$$\nu_{ENDOR} = \left| \frac{1}{h} |m_S| \, W_{shf} \pm \nu_n \mp \frac{1}{h} m_q W_Q \right| \,. \tag{10}$$

In Eqs.(9) and (10):

$$W_{shf} = a + b(3\cos^2\Theta - 1) + b'\sin^2\Theta\cos 2\delta \,, \tag{11}$$

$$W_Q = 3q + (3\cos^2\Theta' - 1) + q'\sin^2\Theta'\cos 2\delta' \,, \tag{12}$$

where Θ, δ and Θ', δ' are the polar angles of B_0 in the principal shf and quadrupole axis system, respectively. The Larmor frequency of a free nucleus in the magnetic field B_0 is

$$\nu_n = \frac{1}{h} g_n \beta_n B_0 \,. \tag{13}$$

The average of the two nuclear magnetic quantum numbers, which are connected by the transition, is

$$m_q = \frac{1}{2}(m_I + m_I') \,. \tag{14}$$

The basic concept for the analysis of ENDOR spectra is briefly reviewed assuming that Eq.(10) holds for frequency position of the ENDOR lines. This is generally not the case since both the anisotropic and quadrupole interactions can become too large with respect to the isotropic term and since g_e-factor anisotropies as well as the fine structure interaction (for $S > 1/2$) can influence the spectra. Most often one needs to diagonalize the spin Hamiltonian numerically, a procedure which has become more and more standard

practice. The identification of the chemical nature of nuclei can be achieved in various ways. According to Eq.(10) for $S = 1/2$ and no quadrupole interaction each nucleus gives a pair of lines separated by $2\nu_n$ if $1/2\,W_{shf} > h\nu_n$ and by W_{shf} if $h\nu_n > 1/2\,W_{shf}$. Since ν_n can be calculated according to Eq.(13) the nuclei can be identified either from the line pairs separated by $2\nu_n$ or by symmetric line patterns about ν_n. If there are several magnetic isotopes present then their line positions must be in the ratios of their respective nuclear moments (if $Q = 0$). The line intensity roughly reflects the isotope abundance. Unfortunately, the ENDOR line intensity is very little understood quantitatively in solids due to the many complicated relaxation paths. Therefore, the two lines, as given by Eq.(10), of each nucleus cannot always be observed, in particular for low frequencies, in stationary ENDOR. However, upon shifting the magnetic field through the ESR line the ENDOR line positions are shifted according to Eq.(10) and Eq.(13). The ENDOR line shift is due to the shift of ν_n and is thus proportional the $g_{n,l}$-value, which is characteristic for a particular nucleus l. If the EPR line width does not allow the measurement of a sufficiently large ENDOR line shift, one can either do additional experiments with a different EPR band or change the resonant frequency of the cavity by inserting material of a suitable dielectric constant and changing the microwave frequency accordingly.

If there is a quadrupole splitting, then each "shf" ENDOR line is split into a characteristic multiplet, e.g., for $I = 3/2$ into a triplet.

To determine the defect structure and the interaction parameters, the dependence of the ENDOR line positions upon variation of the magnetic field orientation with respect to the crystal must be measured and analyzed. This is a major problem in an ENDOR analysis and is an essential tool for the determination of the defect structure.

Figures 3a–3c show such an angular dependence for a cubic crystal such as an alkali halide, calculated according to Eq.(10) for the first three neighbor shells of a defect on a lattice site. The rotation patterns are characteristic of (100), (110) and (111) "symmetry" of the neighbor nuclei. Such a pattern is observed for each m_S-value. From the number of such patterns one can infer the spin of the defect.

Each nucleus has its own principal axis for the shf and quadrupole tensors. Often their orientations in a crystal are determined by symmetry. Otherwise they must be determined from the analysis of the angular dependence of the ENDOR spectra. If the defect center (impurity) and the respective nucleus lie in mirror plane of the defect, then two principal axes must lie in this mirror plane. If the connecting line between the nucleus and the center is a threefold or higher symmetry axis, then the tensor is axially symmetric with its principal axis coincident with this symmetry axis. In practice, one proceeds as follows: one assumes a center model and then calculates the expected angular dependence. Comparison with the experimental angular dependence then verifies or negates the assumption. The symmetry patterns of

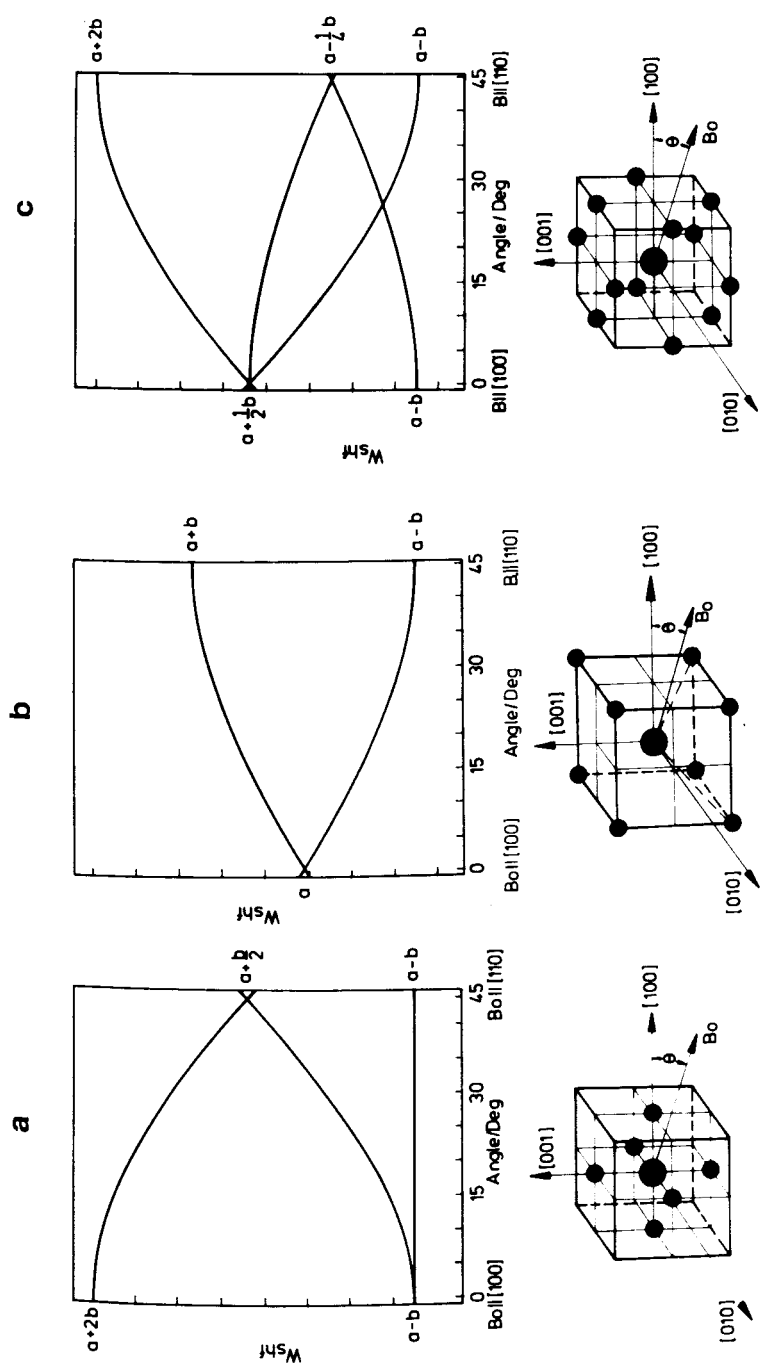

Fig. 3. Calculated ENDOR angular dependence for a substitutional defect in a fcc lattice: **a** — (100)-neighbors; **b** — (111)-neighbors; **c** — (110)-neighbors.

neighbor shells may not be easily recognized, if the first-order solution of the spin Hamiltonian is insufficient. If the agreement between the calculated angular dependence and the experimental one for several planes of rotation is good, the analysis is unambiguously correct. There are many more experimental data points available than parameters to be extracted from them. In a straight ENDOR analysis only the relative signs of the shf constants a, b, b' can be determined. Also the signs of the quadrupole interaction constants with respect to the shf interaction constants are not obtained. With ENDOR-induced ESR and double ENDOR measurements, more information about the signs of the interactions can be extracted from experiment.

Thus, the experimental result is a list of ligand isotopes with their shf and quadrupole interaction constants and the respective orientations of the shf and quadrupole tensors including their symmetry properties. From these results alone one cannot, however, determine the location of the ligands or the paramagnetic impurity. For this, information about the defect wave function is required.

4. Superhyperfine and Quadrupole Interactions

The shf interaction constants are determined by the electronic wave function of the defect and the nuclear moments of the nuclei. The isotropic shf constant of a ligand N_i with coordinate R_{N_i}, is given by

$$a_{N_i} = \frac{2}{3}\mu_0 g_e g_{n,N_i} \beta_e \beta_n (\varrho^{\uparrow}(\vec{R}_{N_i}) - \varrho^{\downarrow}(\vec{R}_{N_i})) , \tag{15}$$

with $\varrho^{\uparrow}$ and $\varrho^{\downarrow}$ the spin-up and spin-down electron densities, respectively. The anisotropic shf constant

$$(b_{N_i})_{k,l} = C \int \frac{(3x_k x_l - r^2)}{r^5} (\varrho^{\uparrow}(\vec{r} + \vec{R}_{N_i}) - \varrho^{\downarrow}(\vec{r} + \vec{R}_{N_i}))\mathrm{d}r^3 , \tag{16}$$

$$C = \frac{\mu_0}{8\pi} g_e g_{n,N_i} \beta_e \beta_n . \tag{17}$$

Finally, the nuclear quadrupole interaction constants are given by Eq.(6). Thus, in principle, the location of all measured nuclei can be obtained, provided $\varrho^{\uparrow}$ and $\varrho^{\downarrow}$ are known. Here lies the major problem. For a number of defects in ionic crystals, approximate wave functions have been calculated, in particular for simple defects such as color centers in alkali halides [6]. However, little such work exists for semiconductors (see Section 6).

5. Atomic Positions in Ionic Crystals

In ionic crystals (crystals with primarily ionic bonding) with large band gaps, the wave function of a point defect decreases monotonically with distance and effects of the valence band play only a minor role (see Section 6). In this case one can often safely assume that the spin density falls off monotonically from the defect center, which at least allows one to assign the measured ligands to particular lattice sites. This consideration can determine the site of the impurity. For example, in alkali halides, atomic hydrogen can occupy both cation and anion vacancy sites as well as interstitial positions. For all three defects, ENDOR has been measured with many ligands [7]. For example, for H^0 occupying an anion vacancy in KCl, the largest spin density is found on the nearest K^+ neighbors (the shf tensor is axial with (100) symmetry), the second largest on Cl^-, which is second nearest neighbor along (110), while for H^0 on cation-vacancy site the largest spin density is found on the nearest Cl^- neighbors (the shf tensor of which is axial with (100) symmetry), the second largest with K^+ along (110). From the experimentally determined equivalence of the ligands (all six nearest neighbors have the same interaction tensors, which are transformed into each other by the symmetry operations about the vacancy), it could be concluded that the H^0 atom is "on-center" in the vacancy. An off-center position would have resulted in splittings in the ENDOR lines. Thus, the sites of H^0 atoms can be determined accurately. However, without a theoretical wave function nothing can be said about lattice relaxations of the H^0 atoms conserving the point group symmetry. For anion-site hydrogen atoms KCl a fairly good wave function has been calculated and lattice relaxations determined [8]. The precision is, of course dependent on the precision of the wave function, and each case has to be judged individually on that basis.

A model wave function, which has been used quite often for simple defects in ionic crystals, is that of an orthogonalized envelope function φ_E [6]. The orthogonalization mixes occupied ligand core orbitals φ_i^α with the envelope function ψ_E, (where the admixture coefficients are the overlap integrals $\langle\psi_E|\varphi_i^\alpha\rangle$), to give

$$\varphi_E = N(\psi_E - \sum_{i,\alpha} \langle\psi_E|\varphi_i^\alpha\rangle\, \varphi_i^\alpha)\,. \tag{18}$$

Here N is a normalization constant such that

$$N^{-1} = (1 - \sum_{i,\alpha} \langle\psi_E|\varphi_i^\alpha\rangle^2)^{1/2}\,. \tag{19}$$

This orthogonalization procedure makes use of the fact that eigenfunctions of the Hamiltonian are orthogonal. For example, in the case of the hydrogen

centers, φ_E could be approximated by the atomic-hydrogen 1s-orbital. Often, covalency effects are included in the admixture coefficient of the nearest neighbors: a covalency parameter is added to the overlap integral, forming an admixture coefficient approximately given by $(\lambda_i^\alpha - \langle\psi_E|\varphi_i^\alpha\rangle)$ [6,9]. In this approximation $\varrho^\uparrow(r) = |\varphi_E(r)|^2$; that is, the complicated many-particle problem is reduced to a one-particle wave function. With the orthogonalized envelope function, it is usually possible to assign a lattice site to the impurity and also to estimate the lattice relaxation. A recent example is that of a defect consisting of a Tl^0 atom next to an anion vacancy along (100) in alkali halides (the so-called $Tl^0(1)$ centers, which are laser active). An estimate of the measured shf interactions with the nearest cations around the vacancy, using an orthogonalized envelope function, predicts that the Tl^0 atom is relaxed by about 10 % of the cation-anion distance towards the vacancy [10]. This value is precise to about ± 30 % due to the approximate character of the wave function.

A more accurate estimate of atomic positions can be made if the interactions with "distant" ligands can be determined with high accuracy by ENDOR. Distant nuclei in that sense have the characteristic feature that their shf interaction constants are $a \approx 0$ or very small, but $b \neq 0$ ($|b| \gg |a|$). Then, the shf interaction can be approximated by the classical point dipole-dipole interaction b^d in which the unpaired electron is replaced by a point dipole at the impurity site:

$$b^d = \frac{\mu_0}{4\pi} g_e \beta_e g_{n,N_i} \beta_n R_{N_i}^{-3}, \tag{20}$$

where R_{N_i} is the distance between the nucleus N_i and the point dipole of the unpaired electron.

An example for the use of the shf interactions of a distant ligand to determine the atomic position of the paramagnetic impurity is that of Ni^+ in CaF_2. In EPR, shf interaction with four equivalent ^{19}F nearest neighbors is resolved, indicating that Ni^+ does not substitute for Ca^{++} at a body-centered site. For this site, eight equivalent ^{19}F neighbors would have been expected, resulting in a 9-line shf EPR pattern. Thus, Ni^+ must have gone off-center such that it has interactions only with four ^{19}F nearest neighbors [11]. With ENDOR the shf interactions with seven shells of ^{19}F neighbors could accurately be determined. Shells 2–6 showed effects of exchange polarization, i.e. negative isotopic shf constants (see below). The shf interactions of shell 7, however, were mostly determined by the classical point dipole-dipole interaction, neglecting overlap effects: $a/h = 0.03$ MHz, $b/h = 0.41$ MHz. $\Theta = 93°$, $\Phi = 90°$, $\Psi = 135°$ (Θ, Φ, Ψ are the Euler angles with respect to the coordinate systems x, y, z in Fig.4, which have to be translated to the respective sites. $\Theta = (\Theta_B, z)$, z_B being the principal axis with the largest interaction). From the orientation of the shf tensor of the shell 7 ^{19}F which in

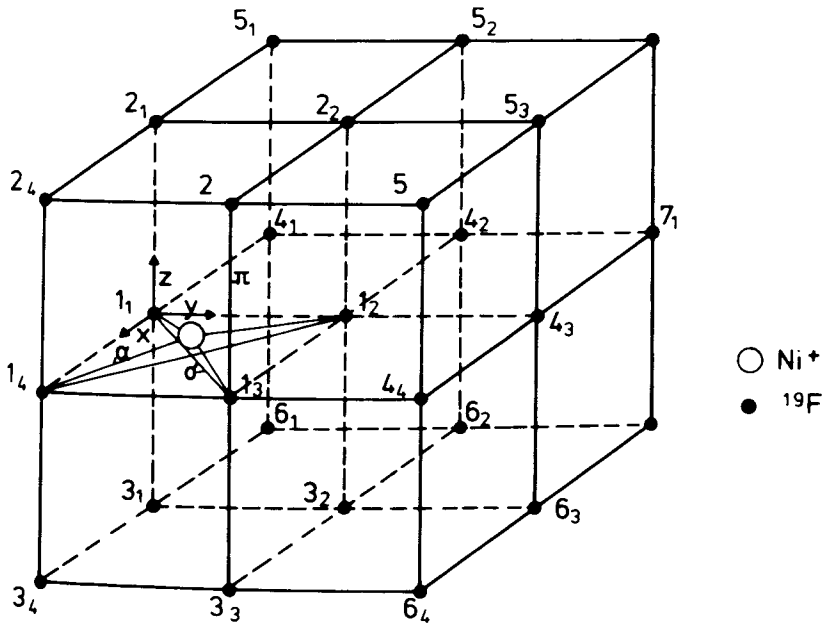

Fig.4. The local environment of the tetragonal Ni^+ center in CaF_2. The numbering of sites refers to the various shells observed by ENDOR. α is the angle between the line connecting Ni^+-$F^{(1)}$ and a face diagonal. The orientation of the shf tensor of ^{19}F in shell 7 is indicated (after [12]).

this case points to the $Ni^+(3d^9)$ point dipole, the position of the Ni^+ ions above the plane constituted by the 4 nearest ^{19}F neighbors could be determined. The angle α (see Fig.4) could be determined from the shell 7 shf tensor orientation to be $\alpha = 9 \pm 3°$ [12]. A lattice relaxation of the distant shell 7 is expected to be small; thus it was not taken into account. Therefore, Ni^+ is slightly off-center, above a plane spanned by 4 F^- ions.

Another example, where the point dipole-dipole interaction could be used to determine the site of a paramagnetic ion is that of Fe^{3+} in $LiTaO_3$ and $LiNbO_3$. Both crystals are of particular interest because of the photorefractive effect, which can be used for the storage of volume phase holograms. This effect is associated with Fe^{3+} impurities. The location of these Fe^{3+} sites has been controversial for a long time. It has been discussed whether it occupies a Li^+ or a Ta^{5+}/Nb^{5+} site [13,14]. In $LiTaO_3$ ENDOR lines with five shells of Li ligands could be measured. Fig.5a represents the Li sublattice assuming Fe^{3+} on a substitutional Ta^{5+} site with Li ligand shells 1 to 5 (with increasing distance from Fe^{3+}), while Fig.5b exhibits the corresponding Li sublattice with the assumption that Fe^{3+} substitutes for Li^+ (Oxygens are not shown for the sake clarity). Figs.6a and 6b show the ENDOR angular dependence (dots) for rotation of the magnetic field in a plane perpendicular to the c-axis of the crystal (z-axis in Figs.5a and 5b). The solid lines are the

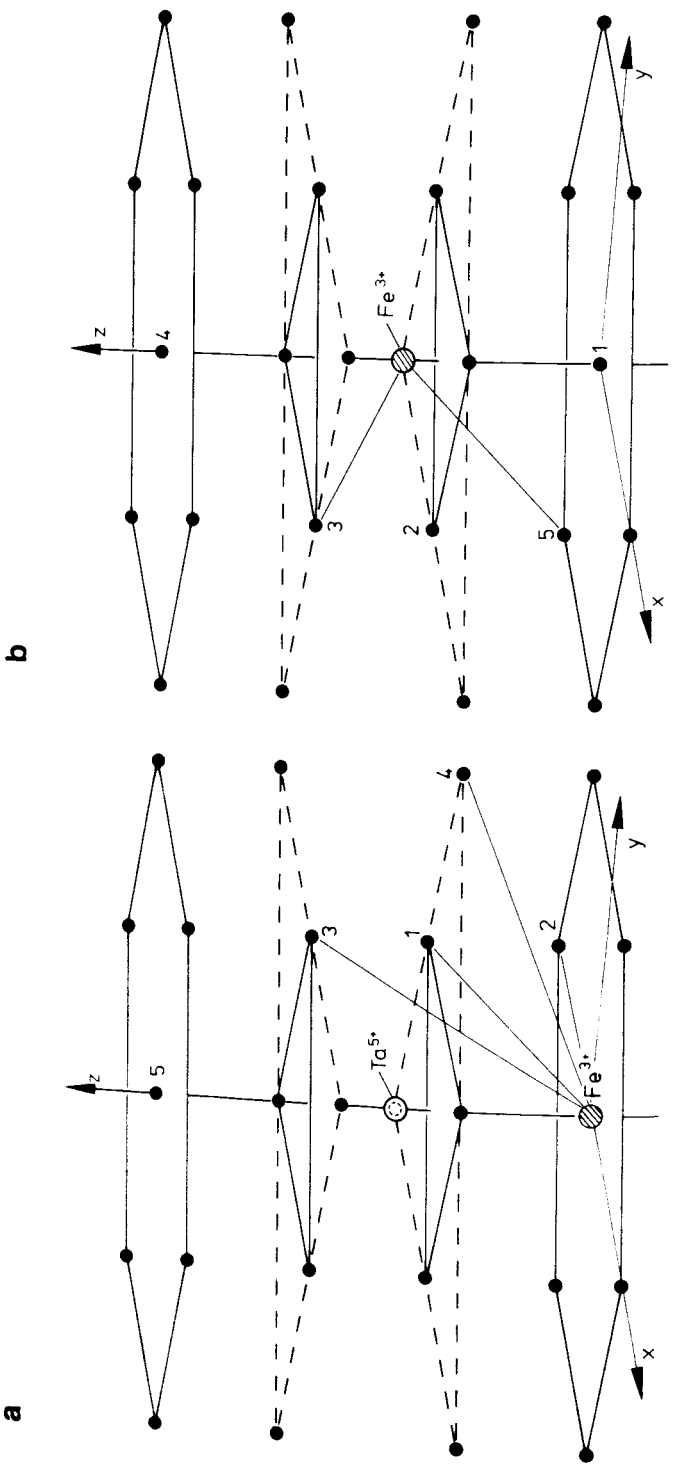

Fig.5. Fe^{3+} sites in $LiTaO_3$. The oxygens are omitted for the sake of clarity. **a** Schematic representation of the Li^+ sublattice assuming Fe^{3+} to be on a substitutional Li site. The numbers 1–5 represent Li shells with increasing distance from the Fe^{3+}. The Ta^{5+} position on the *c*-axis is also indicated (after [15]). **b** Schematic representation of the Li sublattice assuming Fe^{3+} on a substitutional Ta^{5-} site. The numbers 1–5 represent the Li shells with increasing distance from the Fe^{3+} (after [15]).

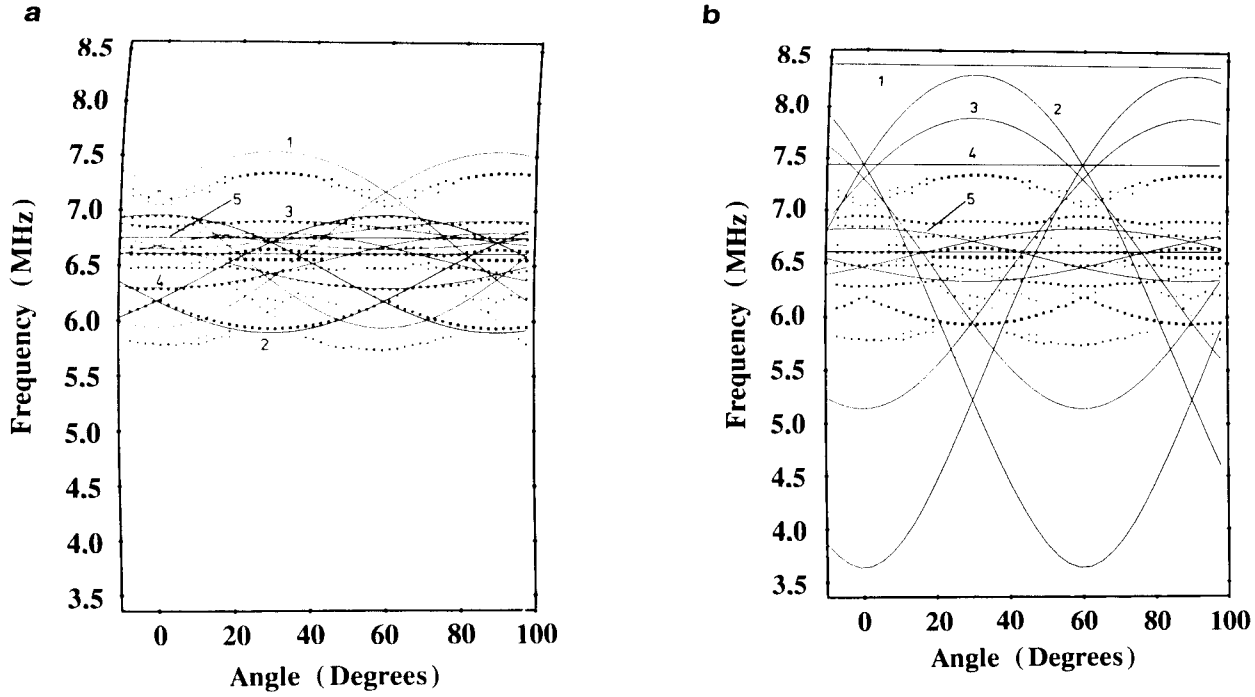

Fig.6. ENDOR of Fe^{3+} centers in $LiTaO_3$ (after [15]). **a** Angular dependence of the Li ENDOR spectra for rotation of the magnetic field in a plane perpendicular to the c-axis. The dots are the experimental line positions. The solid lines represent the calculated angular dependence assuming that the shf interaction is the classical point dipole-dipole interaction for Fe^{3+} occupying a substitutional Li^+ site. The numbers on the branches indicate the Li shells. $0° \triangleq B_0 \| y$-axis, $90° \triangleq B_0 \| x$-axis (see Fig.5a). **b** Angular dependence of the Li ENDOR spectra for rotation of the magnetic field in a plane perpendicular to the c-axis. The dots are the experimental line positions. The solid lines represent the calculated angular dependence assuming that the shf interaction is the classical point dipole-dipole interaction for Fe^{3+} occupying a substitutional Ta^{5+} site. The numbers on the branches indicate the Li shells. $0° \triangleq B_0 \| y$-axis, $90° \triangleq B_0 \| x$-axis (see Fig.5b).

calculated angular dependences assuming classical point dipole-dipole interaction for Fe^{3+} on the Ta^{5+} (Fig.6a) and on the Li^+ site (Fig.6b). There is excellent agreement for shells 2 to 5 assuming a Li^+ site for Fe^{3+}, but none for the Ta^{5+} site. Thus, Fe^{3+} is located on a Li^+ site. Only the nearest Li neighbors have a small isotropic interaction ($a/h = 0.118$ MHz, $b/h = 0.58$ MHz), causing the small disagreement between the calculated and experimental angular dependence in Fig.6b. The calculation did not include the isotropic constant. All other Li ligands have only anisotropic shf interaction with the shf tensors pointing to the Fe^{3+} ion, which is located at the Li^+ site. Fe^{3+} is not off-center along the $\vec{c}$-axis at least to within $\pm$ 0.05 Å. If it was, one would have observed ENDOR line splittings, for instance, from shells 1, 3, 4 above and below the xy plane (Fig.5b). The quoted uncertainty is derived from ENDOR line width [15]. For $LiNbO_3$, very similar results were obtained [16]. If the impurity wave function is rather compact, and if there is little transferred shf interaction [6], then the shf interactions beyond the first few shells are small and almost entirely determined by the classical point dipole-dipole interaction.

Recently, the site of Pb^+ centers could be determined in $KMgF_3$ using ODENDOR. Pb^{++} was doped into $KMgF_3$. Upon X-irradiation at room temperature, Pb^{++} captures an electron and a F^- vacancy moves to the Pb^+ site. One would have expected that Pb^{++} substitutes for Mg^{++}. However, the

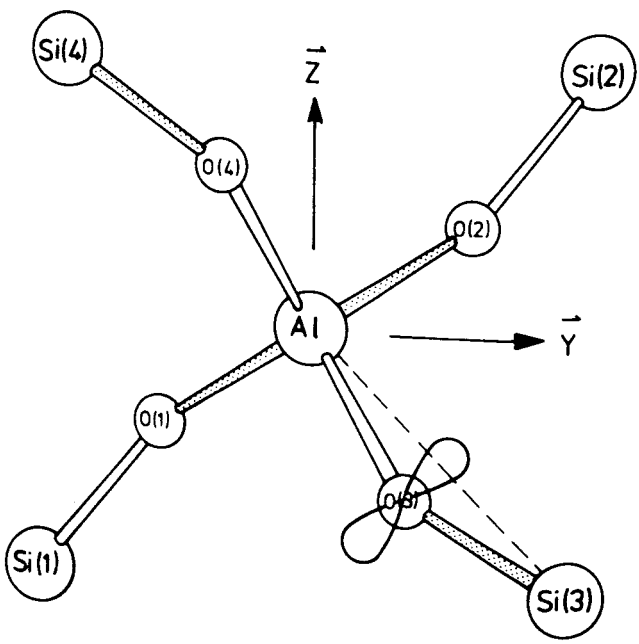

Fig.7. Model of the O^--Al^{3+} center in SiO_2 (after [18,20]). Shorter Si-O bonds are indicated by shading.

analysis of ODENDOR data with four shells of ^{19}F ligands showed that Pb^+ substituted for K^+. It forms two slightly different defects: one with a F^- and a K^+ vacancy pair along [110] as nearest neighbors, and one where the K^+ vacancy pair along [100] while the F^- vacancy remains nearest neighbor along [110] [17]. For the assignment of the neighbors, a wave function of the type of Eq.(18) was used. Since all ^{19}F shf interactions had appreciable isotropic parts, no reasonable estimate could be made about lattice relaxations. For this purpose, the wave function was not known accurately enough.

In a number of oxides such as Al_2O_3 and SiO_2, it was found that for O^- defects (hole centers) the measured anisotropic shf constants with nearest neighbors were considerably smaller than those estimated from the classical point dipole-dipole interaction. It was suggested, that the observed small value was to a large lattice relaxation caused by "bond weakening" and Coulomb repulsion. An increase of the bond length of the regular distance between O^- and Al^{3+} or Si^{++} of up to 40 % was estimated [18,19]. However, in these cases, not only was a small b-value measured, but also a negative isotropic shf constant (the experiment yields only opposite signs for a and b, the choice of sign is based on theory). In these defects there exists a special situation. The unpaired hole is in a p-orbital such that ligands (e.g. Al^{3+}, Si^{4+}) are in a nodal plane of this p-orbital. Fig.7 shows this for the O^--Al^{3+} center in SiO_2. Other examples are O^- centers in Na-β-alumina, GeO_2 and Al_2O_3 [20]. In such a situation, there is no overlap contribution to the anisotropic shf interaction according to Eq.(18), hence the estimate of the lattice relaxation. However, the negative value of a is an indication that exchange polarization effects are to be considered. This was calculated quantitatively for several O^- defects in various oxides considering the following mechanism [20,21]: The unpaired p-orbital in the O^- ion spin polarizes the normally spin-paired 2s- and 2p-orbitals. This spin polarization is then transferred via overlap between the polarized orbitals and the ligands, causing a negative isotropic shf constant, as well as a negative term in the anisotropic shf interaction which largely explains the observed b-values. The exchange polarization term has an exponential dependence on the distance. As a result, only a small relaxation of a few percent has to be assumed to explain the experimental data of the O^- defects considered [20,21]. Recently, with this mechanism to account for the exchange polarization, the shf interaction of an O^- defect residing on a F^- site in BaFBr could also be explained [22].

6. Defects in Semiconductors

The shallow donors P, As and Sb in Si have been investigated by ENDOR [23]. The unpaired electron of shallow donors is highly delocalized as already seen from the simple effective mass theory (EMT). Up to 24 shells of Si ligands could be identified by ENDOR. However, it was not possible to

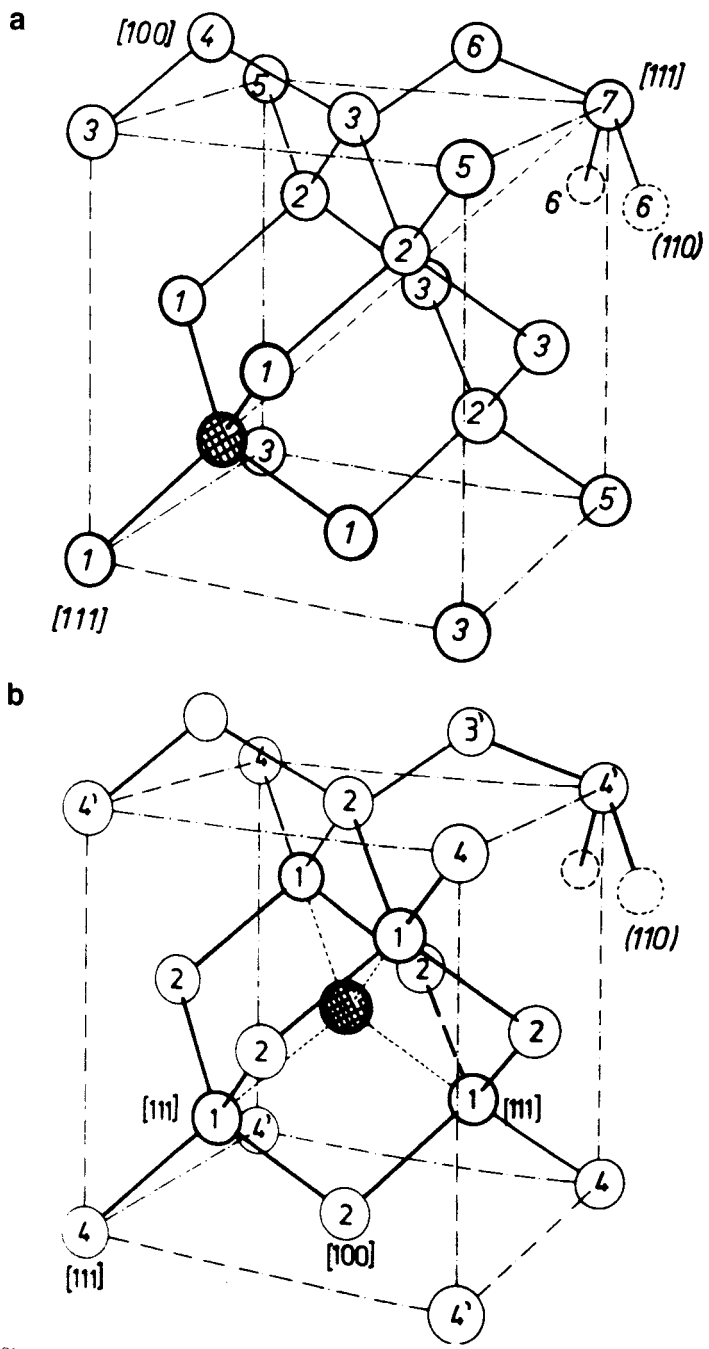

Fig.8. **a** Si lattice with an impurity on a substitutional site. The numbers 1–4 represent the ligand shells with increasing distance from the impurity. Ligands 4 and 4′ have the same distance, but are not equivalent. **b** Si lattice with an impurity on an interstitial site. The numbers 1–7 represent the ligand shells with increasing distance from the impurity.

assign measured shells to particular lattice sites by interpreting the shf data with the usual EMT theory. The spin distribution has an oscillatory character and cannot be described by a monotonically decreasing envelope function. Using a model for the impurity potential, a wave vector-dependent dielectric function representing the screening of the impurity potential by the Si lattice, and pseudopotential Bloch functions, it was possible to assign the shells to specific sites on the basis of theoretical isotropic shf constants [24]. The theory was extended and improved to account for the anisotropic shf interactions also and a satisfactory assignment of experimental ligand shells to nuclear sites could be achieved [25].

From the point of view of atomic positions, the shallow defects are of less interest. This is not so for the so-called deep-level defects, which have energy levels well within the band gap. Their understanding is of current interest both from a fundamental and a technological point of view. The electronic structure cannot be approximated by an "envelope" wave function as discussed in the previous section. In semiconductors the high dielectric constant causes important contributions of the valence bands to the spin density at the ligands. Therefore, the shf interactions cannot be described any more by an impurity wave function alone. One has to deal with a complicated many-electron system, where exchange polarization effects are very important.

In silicon and the III–V compounds, such as GaAs, there is an additional difficulty due to the lattice symmetry. In an ENDOR experiment, one cannot distinguish whether the paramagnetic impurity is substitutional or sitting on an interstitial T_d-site, which has the same (tetrahedral) site symmetry as the substitutional site. As mentioned in Section 3, with ENDOR one can only determine the symmetry types. For the substitutional site the sequence of ligand shells is [111], [110], [110], [100], [110], [110], [111] (see Fig.8, shells 1 to 7). For an interstitial impurity of the T_d-site the sequence is [111], [100], [110], [111], [111], [110], [110] (see Fig.8b). The shf constants do not decrease monotonically with distance and, therefore, the atomic positions of the paramagnetic impurity can only be determined with the help of theory.

ENDOR investigations of chalcogen impurities in Si (S^+, Se^+, and Te^+) serve as an example. Although the interactions of up to 12 Si ligand shells could be determined experimentally, no decision was possible on the chalcogen site [26,27]. A total-energy calculation clearly showed, however, that the substitutional site is energetically more favorable than the interstitial site [28].

It was also for these chalcogen centers in Si that ligand shf interactions were calculated for the first time in a covalent semiconductor. A Green's function technique was used in a spin-unrestricted calculation within the local spin-density approximation [29]. It was shown that the exchange-polarization effects of the valence band had a decisive influence on the shf constants of the ligands. A calculation of the chalcogen pairs [30,31] confirmed the assignment made from the ENDOR experiment that both chalcogens of the pair

occupy substitutional sites [32]. This conclusion was based on the interpretation of the small deviation of the orientation of the (shf) tensor axis of the three nearest Si neighbors of each chalcogen from the ⟨111⟩ axis due to the effect of bonding between the chalcogens. Clearly, such an interpretation relies on assumptions which have to be confirmed by theory.

The effect of valence-band contributions can be quite dramatic and "unexpected" if one assumes that the spin density distribution of a deep-level defect falls off more or less monotonically. Table 1 shows the experimental results of an ENDOR investigation of interstitial Al^{++} defects in Si [33]. The shf interactions of three shells of ligands (see Fig.8b for the notation) are listed as assigned to ligand sites by the experimentalists. They assumed that the largest anisotropic shf interaction should belong to the nearest neighbors (shell 1). A recent calculation using the Green's function technique in the local spin-density approximation, however, showed that the nearest neighbors have a small anisotropic shf constant, the second-nearest ligands with [111] symmetry have a much higher one (Table 1) [33]. Thus, the assignment made by the experimentalist has to be revised. Fig.9 shows the spin-density distribution in the (110) plane (the plane passes through the ligands 4, 2, 4, 4′, 2, 4′ in Fig.8b). The resulting spin density in Si p-orbitals is much higher at the ligands of shell 4 compared to the ligands of shell 1 where the spin distribution is predominantly d-like [34]. If one of the nearest Si neighbors is replaced by Al_s^-, i.e., if Al_i^{++}-Al_s^- pairs are formed, the overall spin density is not drastically perturbed. In particular, the s/d character of the wave function in shell 1 (and hence the small anisotropic shf interaction) is preserved in contrast to the s/p character in shell 4, where the anisotropic shf constant is larger [34], in contrast to the assumption previously made from the experiment [33].

The calculation of nuclear quadrupole interactions not only requires the knowledge of the charge distribution, but also the proper inclusion of the Sternheimer antishielding effects [6]. However, sometimes even a crude estimate can be helpful. One such example is that of Ni^{3+} ($3d^7$) in GaP. The quadrupole interactions measured with Ga ligands were rather small

Table 1. Superhyperfine interactions of three shells of ^{29}Si ligands of Al_i^{++} centers in Silicon.

^{29}Si-shell	Type	a/h exp.	a/h theor.	b/h exp.	b/h theor.
1	⟨111⟩	52.31	54.7	3.91	0.76
4,4′	⟨111⟩	50.09	51.6	−0.05	5.24
2	⟨100⟩	22.6	32.8	1.14	2.2

Note: All shf interactions in MHz. Experimental values after [33], theoretical values after [34].

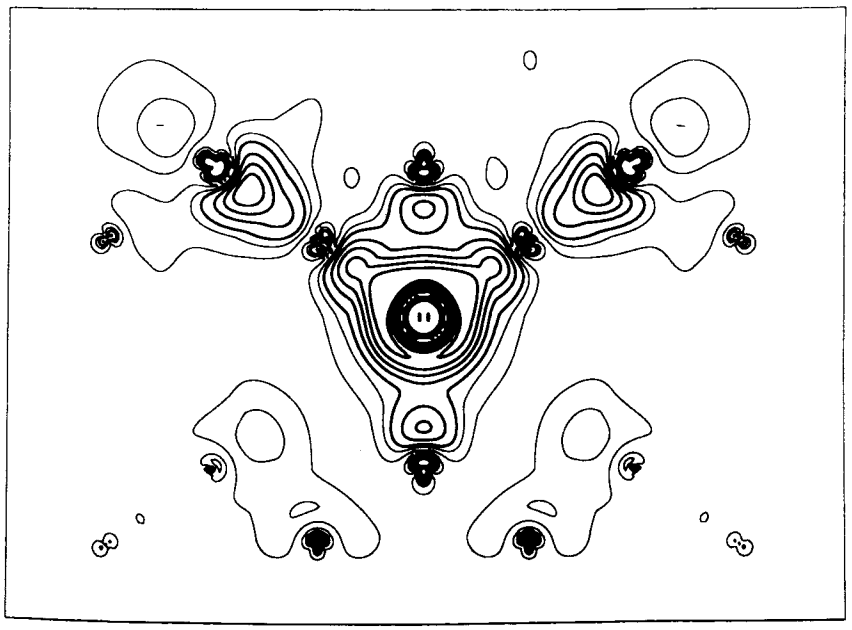

Fig.9. Contour plot of the particle density of the gap state of Al_i^{++} in the (110) plane. The Al atom is at the center of the figure. The Si ligands can be identified from the oscillations of the particle density in the core regions (after [34]).

(q/h (^{71}Ga) = 0.018 MHz). If Ni^{3+} substituted for Ga, no large electric field gradient on the nearest Ga ligand site would be expected, since Ni^{3+} is bonded like Ga^{3+} (in the ionic limit). However, if Ni^{3+} were interstitial, a q/h of 0.45 MHz would be expected for the ^{71}Ga ligand from a point-charge estimate, according to Eq.(6). Thus, in this case, such a simple estimate can help to determine the atomic position [35].

To conclude this section, in semiconductors simple approximations usually break down and the determination of atomic positions as well as the assignment of ligands to the experimental shf tensors are generally not possible without a proper theory.

7. Dynamic Effects

Dynamic effects on atomic positions are often seen in ENDOR due to its high resolution power for shf interactions. They are mostly observed as a temperature dependence of shf interactions. Upon increase of temperature the lattice expansion will mostly cause a decrease of the shf interactions in ionic crystals, which is the result of the superposition of two opposite effects: the increasing distance between impurity and ligands results in a de-

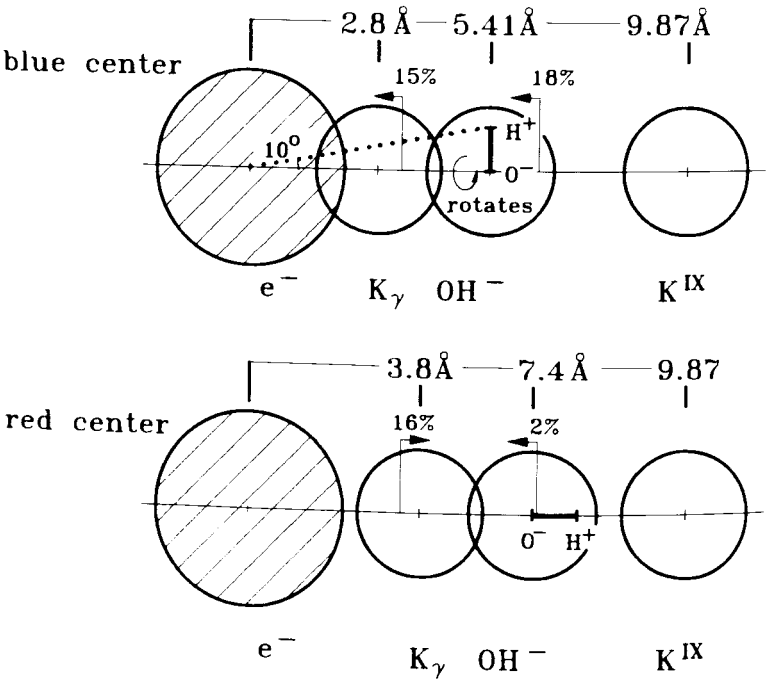

Fig.10. Structure models of the "blue" and "red" $F_H(OH)^-$ aggregate centers in KBr (see text after [38]).

crease of shf interactions and the increase of lattice-vibration amplitudes results in a slight increase of overlap contributions to the shf interactions. However, for light impurities such as atomic hydrogen the net effect is positive: the thermally activated localized vibration of the light paramagnetic atom leads to increased overlap admixtures of ligand orbitals and thus to an increase of the shf interactions [7].

A low-symmetry configuration of a defect such as an off-center position of an impurity frozen in at low temperature may undergo a thermally activated motion upon increase of the temperature. The impurity can quickly jump over several low temperature sites, which results in the observation of a thermally averaged EPR or ENDOR spectrum. There are many such examples in the literature.

ENDOR spectra of a paramagnetic defect in a crystal which undergoes a structural phase transition will reflect the change of symmetry at the phase transition. For example, Mn^{2+} was studied in $RbCdF_3$ above and below the transition from the cubic to the tetragonal phase at 124 K. From ENDOR the "order parameter" for this transition could be determined as a function of temperature since this parameter represents the rotation of MnF_6 octahedra about a cubic axis when undergoing the phase transition. The rotation angle is the angle of the ^{19}F shf tensors of the nearest neighbors [36].

Recently, another dynamical effect on atomic positions became apparent where the entropy content of a defect determines its microscopic structure and its changes upon temperature variation. In alkali halides the so-called F-center, which consists of an electron trapped at an anion vacancy site, can from pair defects with OH^- dipoles substituting for halide ions. It was discovered by optical investigations that in KBr these $F_H(OH)^-$ aggregate defects have a thermal and optical bistability. Their configuration at high temperature (150 K) is different from that at low temperature (4 K) as concluded from the changes of the optical absorption bands [37]. The high-temperature configuration was called "red" center, from the red shifted absorption band compared to the isolated F^- center, the low temperature configuration accordingly "blue" center, due to the blue shift of its absorption band. With ENDOR the microscopic structure of the two configurations could be determined (Fig.10). In both centers, the OH^- ion does not occupy the nearest possible site (110), but a (200) 4th shell position. In the red center the proton shf interaction constant has a small isotropic and a larger anisotropic part. The latter can be approximated by the classical point dipole-dipole interaction rather well (see Section 4). The proton position could thus be determined (see Fig.10). In the red center the OH^- dipole is along a [100] axis in the orientation shown in Fig.10. In the blue center the proton shf interaction also has [100] axial symmetry due to tunneling between the four possible positions, one of which is indicated in Fig.10. The isotropic shf constant has a small negative value ($a/h = -0.14$ MHz) associated with a larger anisotropic value ($b/h = 0.47$ MHz). The negative a-value is due to exchange polarization. Analysis of the two shf constants yielded the "perpendicular" position of the OH^- dipole shown in Fig.10 [38]. The question arose as to why the blue center transforms into the red one upon raising the temperature. In KCl such a bistability is not observed, only the red-center configuration exists [38]. In KCl it was observed, however, that the proton shf interaction of the OH^- dipole is strongly temperature dependent. It increases with increasing temperature. The OH^- dipole has localized vibrations along the (100) axis with large amplitudes in a shallow anharmonic potential. Such vibrations exist also in KBr, but could not be followed as well as by ENDOR in KCl. Considering the dynamic properties of the OH^- dipoles the bistability was explained by taking the entropy into account following a suggestion made for unknown defects in electron-irradiated Si [39]. Instead of discussing the internal energy one has to consider the Gibbs free energy, which is given by

$$G = H - TS, \tag{21}$$

where H is the configurational enthalpy, T is the temperature and S is the entropy. For $T = 0$ there is no influence of the entropy term. At $T = 0$ (or low temperature) apparently G is lower for the blue center than for the red one. Due to the anharmonic OH^--vibration in the red center, its entropy is

larger than that of the blue center, which is $S = k_B \ln 4$ from the four equivalent perpendicular OH^- orientations between which the tunneling occurs. Thus, for a sufficiently high temperature

$$\Delta G = G_{red} - G_{blue} = (H_{red} - H_{blue}) - T(S_{red} - S_{blue}) < 0 . \quad (22)$$

This means that at sufficiently high temperature G_{red} is less than G_{blue}, i.e. the red configuration becomes the most probable one. This was also shown quantitatively in [38].

8. Conclusions

In ionic crystals, atomic positions can be accurately determined if ENDOR data are available for distant ligands which show only the classical point dipole-dipole interaction. Therefore, it pays also to analyze the small interactions in the ENDOR spectra, that is those of distant nuclei. They can be more important than the shf interactions of nearer neighbors for structure determination. The defect wave function can often be approximated rather well by the orthogonalized envelope function, including covalency effects. On the other hand, in semiconductors, the determination of atomic positions is very difficult and probably mostly misleading without a proper theory. A question still open is that of lattice relaxation in semiconductors. No calculations of ligand hyperfine interactions taking lattice relaxations into account for defects in Si or in III–V compounds have been done.

Acknowledgement

The author is grateful for many helpful discussions with Prof. Dr. H.Overhof.

References

[1] Seidel H.: Z. Phys. **165**, 239 (1961)
[2] Spaeth J.-M., Lohse F.: J. Phys. Chem. Sol. **51**, 861 (1990)
[3] Spaeth J.-M.: Experimentelle Technik der Physik, **36**, 257 (1988)
[4] Mollenauer L.F., Pan S.: Phys. Rev. B **6**, 772 (1972)
[5] Spaeth J.-M., Koschnick F.K.: J. Phys. Chem. Sol. **52**, 1 (1991)
[6] Stoneham A.M.: Theory of Defects in Solids. Oxford: Clarendon Press 1975.
[7] Spaeth J.-M. in: Defects in Insulating Crystals (Tuchkevich V.M., Shvartz K.K., eds.). p.232. New York, Heidelberg: Springer 1981.
[8] Heder G., Spaeth J.-M., Harker A.H.: J. Phys. C: Solid State Phys. **13**, 4965 (1980)
[9] Spaeth J.-M., Seidel H.: phys. stat. sol. **46**, 323 (1971)

[10] Ahlers F.J., Spaeth J.-M.: J. Phys. C: Solid State Phys. **19**, 4693 (1986)
[11] Casas-Gonzáles J., den Hartog A.W., Alcalá R.: Phys. Rev. B **21**, 3826 (1980)
[12] Studzinski P., Casas-Gonzáles J., Spaeth J.-M.: J. Phys. C: Solid State Phys. **17**, 5411 (1984)
[13] Agulló-López F., Müller K.A.: Crystl. Latt. Defect and Amorph. Materials **15**, 89 (1987)
[14] Keune W., Dale S.K., Gonser U., Bunzel H.: Ferroelectrics **13**, 443 (1976)
[15] Söthe H., Rowan L.G., Spaeth J.-M.: J. Phys. Condensed Matter **1**, 3591 (1989)
[16] Söthe H., Spaeth J.-M.: to be published.
[17] Fockele M., Lohse F., Spaeth J.-M.: Israel Journal of Chemistry **29**, 13 (1989)
[18] Schirmer O.F.: Solid State Commun. **18**, 1349 (1976)
[19] Stapelbroek M., Gilliam R.O., Bartram R.H.: Phys. Rev. B **16**, 37 (1977)
[20] Adrian F.J., Jette A.N., Spaeth J.-M.: Phys. Rev. B **31**, 3923 (1985)
[21] Adrian F.J., Jette A.N., Spaeth J.-M.: J. Phys. C: Solid State Phys. **19**, L331 (1986)
[22] Koschnick F., Spaeth J.-M.: to be published.
[23] Mieher R.L., Hale E.B.: Phys. Rev. **184**, 739 (1969)
[24] Ivey J.L., Mieher R.L.: Phys. Rev. B **11**, 822 (1975)
[25] Ivey J.L., Mieher R.L.: Phys. Rev. B **11**, 849 (1975)
[26] Niklas J.R., Spaeth J.-M.: Solid State Commun. **46**, 121 (1983)
[27] Greulich-Weber S., Niklas J.R., Spaeth J.-M.: J. Phys. C: Solid State Phys. **17**, L911 (1984)
[28] Beeler F., Scheffler M., Jepson O., Gunnarson O.: Proceedings of the Conference of the Material Research Society Annual Meeting, San Francisco **46**, 117 (1985)
[29] Overhof H., Scheffler M., Weinert C.M.: Mat. Sci. Forum **38-41**, 293 (1989)
[30] Overhof H., Scheffler M., Weinert C.M.: Mat. Sci. and Eng. **4**, 315 (1989)
[31] Overhof H., Scheffler M., Weinert C.M.: Phys. Rev. B **43**, 12494 (1991)
[32] Greulich-Weber S., Niklas J.R., Spaeth J.-M.: J. Phys. Condensed Matter **1**, 35 (1989)
[33] Niklas J.R., Spaeth J.-M., Watkins G.D.: Proceedings of the Materials Research Society Conference, San Francisco **46**, 237 (1985)
[34] Overhof H., Corradi G.: Proceedings of the 16th International Conference on the Physics of Defects in Semiconductors, Bethlehem, PA, 1991.
[35] Ueda Y., Niklas J.R., Spaeth J.-M., Kaufmann U., Schneider J.: Solid State Commun. **46**, 127 (1983)
[36] Studzinski P., Spaeth J.-M.: J. Phys. C: Solid State Phys. **19**, 6441 (1986)
[37] Baldacchini C., Botti S., Grassano U.M., Gomes L., Lüty F.: Europhysics Lett. **9**, 735 (1989)
[38] Söthe H., Spaeth J.-M., Lüty F.: Rev. of Solid State Sci. **4**, 499 (1990)
[39] Hamilton B., Peaker A.P., Pantelides S.T.: Phys. Rev. Lett. **61**, 1627 (1988)

Author's address: Prof. Dr. Johann-Martin Spaeth, Fachbereich Physik, Universität-GH Paderborn, Warburger Straße 100, D-4790 Paderborn, Germany